



# Diffusion-driven magnesium and iron isotope fractionation in Hawaiian olivine

Fang-Zhen Teng <sup>a,\*</sup>, Nicolas Dauphas <sup>b</sup>, Rosalind T. Helz <sup>c</sup>, Shan Gao <sup>d,e</sup>, Shichun Huang <sup>f</sup>

<sup>a</sup> Isotope Laboratory, Department of Geosciences and Arkansas Center for Space and Planetary Sciences, University of Arkansas, 113 Ozark Hall, Fayetteville, AR 72701, USA

<sup>b</sup> Origins Laboratory, Department of the Geophysical Sciences and Enrico Fermi Institute, The University of Chicago, 5734 South Ellis Avenue, Chicago, IL 60637, USA

<sup>c</sup> U.S. Geological Survey, Reston, VA 20192, USA

<sup>d</sup> State Key Laboratory of Geological Processes and Mineral Resources, Faculty of Earth Sciences, China University of Geosciences, Wuhan 430074, China

<sup>e</sup> State Key Laboratory of Continental Dynamics, Northwest University, Xi'an 710069, China

<sup>f</sup> Department of Earth and Planetary Sciences, Harvard University, 20 Oxford Street, Cambridge, MA 02138, USA

## ARTICLE INFO

### Article history:

Received 17 February 2011

Received in revised form 31 May 2011

Accepted 2 June 2011

Available online 28 June 2011

Editor: R.W. Carlson

### Keywords:

magnesium isotopes

iron isotopes

chemical diffusion

olivine

zoning

Hawaii

## ABSTRACT

Diffusion plays an important role in Earth sciences to estimate the timescales of geological processes such as erosion, sediment burial, and magma cooling. In igneous systems, these diffusive processes are recorded in the form of crystal zoning. However, meaningful interpretation of these signatures is often hampered by the fact that they cannot be unambiguously ascribed to a single process (e.g., magmatic fractionation, diffusion limited transport in the crystal or in the liquid). Here we show that Mg and Fe isotope fractionations in olivine crystals can be used to trace diffusive processes in magmatic systems. Over sixty olivine fragments from Hawaiian basalts show isotopically fractionated Mg and Fe relative to basalts worldwide, with up to 0.4‰ variation in  $^{26}\text{Mg}/^{24}\text{Mg}$  ratios and 1.6‰ variation in  $^{56}\text{Fe}/^{54}\text{Fe}$  ratios. The linearly and negatively correlated Mg and Fe isotopic compositions [i.e.,  $\delta^{56}\text{Fe} = (-3.3 \pm 0.3) \times \delta^{26}\text{Mg}$ ], co-variations of Mg and Fe isotopic compositions with Fe/Mg ratios of olivine fragments, and modeling results based on Mg and Fe elemental profiles demonstrate the coupled Mg and Fe isotope fractionation to be a manifestation of Mg–Fe inter-diffusion in zoned olivines during magmatic differentiation. This characteristic can be used to constrain the nature of mineral zoning in igneous and metamorphic rocks, and hence determine the residence times of crystals in magmas, the composition of primary melts, and the duration of metamorphic events. With improvements in methodology, in situ isotope mapping will become an essential tool of petrology to identify diffusion in crystals.

© 2011 Elsevier B.V. All rights reserved.

## 1. Introduction

Understanding the mechanisms of isotope fractionation is a prerequisite for using stable isotopes as tracers of geological processes. For example, the isotope fractionation associated with changes in Fe oxidation may be used to estimate the oxygen fugacity of mantle reservoirs (Dauphas et al., 2009a; Williams et al., 2004, 2005). Recent experimental studies furthermore found large Fe isotope fractionation associated with diffusion of Fe along chemical and temperature gradients (Richter et al., 2009a). Thus, Fe isotopes could potentially be used as geospeedometers or tracers of temperature variations. However, it is difficult to evaluate the extent to which these different processes can affect Fe isotopic variations in natural systems. For example, previous studies on Fe isotopes in Kilauea Iki lava lake revealed large Fe isotope fractionation in bulk rocks and separated olivine fragments (Teng et al., 2008). These isotopic variations have been interpreted to result either from equilibrium isotope fractionation enhanced by chromatographic effects

(possibly associated with the change of oxidation state of Fe) or from diffusion-driven kinetic isotope effects.

$\text{Mg}^{2+}$  and  $\text{Fe}^{2+}$  have identical charges and similar ionic radii, so they behave similarly during partial melting and magmatic differentiation. Therefore, coupled studies of Fe and Mg isotopes could help identify the processes that are responsible for Fe isotope fractionation, as changes in redox conditions does not fractionate Mg isotopes whereas chemical and Soret diffusion will fractionate Fe and Mg isotopes in predictable ways (Dauphas, 2007; Huang et al., 2010; Richter et al., 2008, 2009b; Roskosz et al., 2006).

To evaluate the mechanisms governing high-temperature fractionation of stable isotopes, we analyzed Mg and Fe isotopes as well as Fe/Mg ratios for olivine fragments separated from Kilauea Iki lava lake, Loihi and Koolau volcanoes, Hawaii. Our results demonstrate up to 0.4‰ fractionation of Mg isotopes and 1.6‰ fractionation of Fe isotopes during Mg–Fe inter-diffusion in zoned olivines during magmatic differentiation.

## 2. Samples

Kilauea Iki lava lake formed during the 1959 summit eruption of Kilauea volcano by filling a previously existing crater (Helz, 1987a).

\* Corresponding author.

E-mail address: [fteng@uark.edu](mailto:fteng@uark.edu) (F.-Z. Teng).

Olivine collected by drilling cores from the Kilauea Iki lava lake are all normally zoned, may vary by 5% Fo [Fo = molar  $100 \times \text{Mg} / (\text{Mg} + \text{Fe})$ ] or more, and have re-equilibrated with the melt during slow cooling (Helz, 1987b). Olivine fragments from Kilauea Iki lava lake studied here for Mg isotopes and Fe/Mg ratios are the same as those used in a previous study of Fe isotopes (Teng et al., 2008). Olivine fragments were picked up from two drill core samples. One drill core sample was quenched at relatively high temperature (KI81-5-254.5, 1134 °C) and the other one was quenched at relatively low temperature (KI75-1-139.3, 1070 °C) (Teng et al., 2008).

Olivine fragments were also separated from basalt samples from Koolau Volcano and Loihi seamount, Hawaii. Olivines from Koolau volcano are fragments mainly from a single large olivine phenocryst in a tholeiitic basalt specimen, with a diameter of 2 mm. Olivines from Loihi seamount are fragments of multiple olivine phenocrysts in one alkaline basalt hand specimen. These olivine fragments were analyzed for both Mg and Fe isotopes, as well as Fe/Mg ratio. Whole-rock basalt samples, from which olivine fragments were separated, were analyzed for Fe isotopes. Their Mg isotopic compositions were shown by Teng et al. (2007, 2010a) to be homogenous.

### 3. Analytical methods

#### 3.1. Mineral analysis

Major element compositions of olivines in two drilled core samples from Kilauea Iki lava lake were analyzed on a JEOL JXA-8100 SuperProbe Electron Probe Microanalyzer (EPMA) at the State Key Laboratory of Geological Processes and Mineral Resources, China University of Geosciences (Wuhan), using an accelerating voltage of 15 kv, beam current of 10 nA and spot diameter of 1  $\mu\text{m}$  on polished thin sections. Calibration of elemental analyses was done using multiple silicate and pure oxide standards from SPI Supplies, Inc., USA.

#### 3.2. Iron isotope analysis

Pure olivine fragments were handpicked under a binocular microscope, cleaned with Milli-Q water for  $3 \times 10$  min in an ultrasonic bath, and dried under a heat lamp before dissolution. Both whole-rock basalt powders and olivine fragments were dissolved in a combination of HF–HClO<sub>4</sub>–HNO<sub>3</sub>. Iron was purified on anion exchange resin (AG1-X8 200–400 mesh) in HCl medium using established procedures (Dauphas et al., 2004, 2009b). Its isotopic composition was analyzed with a Neptune high-resolution MC-ICPMS installed at the Origins Laboratory of the University of Chicago. Iron isotope data are reported in standard  $\delta$ -notation in per mil deviation relative to the composition of IRMM-014:  $\delta^X\text{Fe} = [({}^X\text{Fe}/{}^{54}\text{Fe})_{\text{sample}} / ({}^X\text{Fe}/{}^{54}\text{Fe})_{\text{IRMM-014}} - 1] \times 1000$ , where X refers to 56 or 57. Total procedure blank was <20 ng and is negligible compared to Fe loaded on the column (~100  $\mu\text{g}$  of Fe). The long-term precision, based on replicate analyses of granites, basalts, and chondrites, is  $\pm 0.03\%$  ( $\delta^{56}\text{Fe}$ , 95% confidence interval) (Dauphas et al., 2009b; Teng et al., 2008).

#### 3.3. Magnesium isotope analysis

Magnesium isotopic analyses were performed at the Isotope Laboratory of the University of Arkansas, Fayetteville, following previously established procedures (Li et al., 2010; Liu et al., 2010; Teng et al., 2010a, 2010b; Yang et al., 2009). In brief, digested olivine solutions used for Fe isotopic studies were dried down and re-dissolved in 1 M HNO<sub>3</sub>. Separation of Mg was achieved by cation exchange chromatography with Bio-Rad 200–400 mesh AG50W-X8 resin in 1 M HNO<sub>3</sub>. Samples containing ~50  $\mu\text{g}$  of Mg were loaded on the resin and Mg was eluted with 1 M HNO<sub>3</sub>. Magnesium isotopic compositions were analyzed by the standard bracketing method using a Nu Plasma MC-ICP-MS at the University of Arkansas. Magnesium isotope data are reported in

$\delta$ -notation in per mil relative to DSM3:  $\delta^X\text{Mg} = [({}^X\text{Mg}/{}^{24}\text{Mg})_{\text{sample}} / ({}^X\text{Mg}/{}^{24}\text{Mg})_{\text{DSM3}} - 1] \times 1000$ , where X refers to 25 or 26. Total procedure blank was <10 ng and is negligible compared to Mg loaded on the column. The long-term precision, based on replicate analyses of synthetic solutions, mineral and rock standards, is  $\pm 0.07\%$  ( $\delta^{26}\text{Mg}$ , 2SD) (Teng et al., 2010a).

#### 3.4. Fe/Mg ratio analysis

Fe/Mg ratios of the olivine samples were measured using the same dissolutions on a GV Platform XS Quadrupole ICP-MS at Harvard University. In detail, aliquots of the olivine solutions were diluted by a factor of 5000 in 1.5% HNO<sub>3</sub>. Peaks of <sup>24</sup>Mg, <sup>25</sup>Mg, <sup>26</sup>Mg and <sup>57</sup>Fe were scanned. Instrumental background was measured on a 1.5% HNO<sub>3</sub> solution. Most polyatomic interferences, such as <sup>12</sup>C<sup>14</sup>N and <sup>40</sup>Ar<sup>16</sup>O<sup>1</sup>H, were removed by the collision cell on the GV Platform XS ICP-MS, and the background correction for all measured samples and standards was less than 2%. The measured <sup>57</sup>Fe/<sup>24</sup>Mg, <sup>57</sup>Fe/<sup>25</sup>Mg and <sup>57</sup>Fe/<sup>26</sup>Mg ratios were then converted to Fe/Mg weight ratios using a calibration curve obtained by measuring the solutions of three USGS standard samples, BHVO-1, BCR-1 and AGV-1. Each olivine sample was analyzed twice. A solution of BHVO-2 was analyzed as an unknown during the course of analysis, and four independent measurements yielded Fe/Mg ratios of 1.965, 1.962, 1.957 and 1.946, with an average value of  $1.958 \pm 0.017$  (2 SD). The relative uncertainty of these four independent Fe/Mg measurements,  $\pm 0.9\%$ , is used as the relative uncertainty of Fe/Mg in all analyzed olivine solutions. This  $\pm 0.9\%$  relative uncertainty in Fe/Mg translates into an uncertainty of  $\pm 0.2$  in the calculated Fo content.

#### 3.5. Modeling of diffusion-driven Mg–Fe isotope fractionations in olivine

Diffusive exchange of Mg and Fe in olivine from sample KI81-5-254.5 in Kilauea Iki lava lake was modeled by modifying a Mathematica code developed by Dauphas et al. (2010). The Mg–Fe inter-diffusion coefficient depends on temperature (T), pressure (P), Fo content, and oxygen fugacity following the parameterization of Dohmen and Chakraborty (2007). The crystallographic orientation was not taken into account, as this was unknown for the measured profiles. The  $f\text{O}_2$  was taken to be at NNO-0.5 (Helz and Thornber, 1987) and its absolute value was calculated at any P and T using the parameterizations of Huebner and Sato (1970), Chou (1987), and Herd (2008). We assumed an initial temperature of the lava lake in 1959 of 1190 °C (Helz, 2009). The sample was recovered in 1981 at a temperature of ~1100 °C (Barth et al., 1994) representing the quenching temperature  $T_q$ . The ratio of diffusivities of isotopes was expressed as  $D_2/D_1 = (m_1/m_2)^\beta$ , where  $\beta$  is ~0.05 for Mg and Fe in silicate melts (Richter et al., 2009b). The values are not known for olivine so the values for silicate melts were used here instead. The temperature at any given depth [T(t)] was assumed to vary with time (t) as  $T(t) = T_0 \operatorname{erf} \sqrt{\tau} / t$ , where  $T_0$  is the initial temperature of the lava lake and  $\tau$  is the cooling timescale and is the only adjustable parameter of the model. This equation corresponds to cooling of a semi-infinite solid at constant initial temperature  $T_0$  and zero surface temperature. The Fo content of the initial olivine is Fo86 (Helz, 1987b). The Fo content of the olivine at the contact with magma (rim) was assumed to vary linearly with temperature between  $T_0$  and  $T_q$  following fractional crystallization of the lava lake. The initial rim Fo content was Fo86 and the final one was that measured in the profile (e.g., ~Fo71 for olivine II). Given the spherical symmetry of the system, a no-flux boundary condition was imposed at the center of olivine and only half of it was modeled. The cooling timescale  $\tau$  was adjusted so as to reproduce the Fo content of the final olivine core (~Fo80 for olivine II).

## 4. Results

Magnesium and iron isotopic compositions as well as Fo contents of olivine fragments are reported in Table 1. Magnesium and Fe isotopic

**Table 1**  
Magnesium and iron isotopic compositions of olivine fragments from Hawaii basalts.

Sample	wt. (mg)	Fo	n	$\delta^{56}\text{Fe}$ (‰)	95% c.i.	$\delta^{57}\text{Fe}$ (‰)	95% c.i.	$\delta^{25}\text{Mg}$ (‰)	2 SD	$\delta^{26}\text{Mg}$ (‰)	2 SD
<i>KI81-5-254.5</i>											
Ol-1	0.56		9	-0.755	0.032	-1.112	0.044				
Ol-2	0.72		9	-0.721	0.032	-1.078	0.044				
Ol-3	0.24		9	+0.032	0.032	+0.007	0.044				
Ol-4	0.37		9	-0.073	0.032	-0.110	0.044				
Ol-5	0.71		9	+0.005	0.032	+0.010	0.044				
Ol-6	0.84		9	-0.134	0.032	-0.225	0.044				
Ol-7	0.60		9	-0.079	0.032	-0.139	0.044				
Ol-8	0.96	81.5	9	-0.056	0.044	-0.108	0.068	-0.09	0.06	-0.23	0.07
Ol-9	0.34	81.0	9	+0.085	0.044	+0.104	0.068	-0.13	0.06	-0.28	0.07
Ol-10	0.49	80.7	9	+0.038	0.044	+0.066	0.068	-0.14	0.06	-0.29	0.07
Ol-11	1.24	83.0	9	-0.683	0.044	-1.023	0.068	-0.04	0.06	-0.07	0.07
Replicate								-0.04	0.06	-0.07	0.06
Ol-12	0.72	83.9	9	-1.103	0.033	-1.680	0.067	0.03	0.06	0.03	0.07
Replicate								0.02	0.06	0.02	0.09
Ol-13	0.42	81.0	9	+0.035	0.033	+0.039	0.067	-0.12	0.06	-0.27	0.07
Replicate								-0.14	0.07	-0.28	0.06
Ol-14	0.26	80.8	9	+0.032	0.033	+0.029	0.067	-0.15	0.06	-0.26	0.07
Ol-15	0.48	82.1	9	-0.419	0.033	-0.620	0.067	-0.09	0.06	-0.17	0.08
Ol-16	0.46	80.9	9	+0.067	0.033	+0.083	0.067	-0.17	0.06	-0.32	0.08
Ol-17	0.53	80.3	9	+0.041	0.033	+0.045	0.067	-0.14	0.05	-0.30	0.06
Ol-18	0.67	81.3	9	-0.154	0.033	-0.236	0.067	-0.12	0.05	-0.20	0.06
Ol-19	0.41	81.9	9	-0.420	0.034	-0.629	0.060	-0.05	0.06	-0.13	0.07
Ol-20	1.02	81.2	9	-0.085	0.034	-0.149	0.060	-0.12	0.06	-0.23	0.07
Ol-21	1.42	80.9	9	+0.022	0.034	+0.014	0.060	-0.15	0.06	-0.27	0.06
<i>KI75-1-139.3</i>											
Ol-1	0.75		9	-0.253	0.032	-0.406	0.044				
Ol-2	0.47		9	-0.149	0.032	-0.284	0.044				
Ol-3	0.69		9	-0.412	0.032	-0.634	0.044				
Ol-4	0.79		9	+0.017	0.032	-0.137	0.044				
Ol-5	0.49		9	-0.212	0.032	-0.341	0.044				
Ol-7	0.43		9	-0.319	0.032	-0.507	0.044				
Ol-8	2.72		9	-0.164	0.032	-0.294	0.054				
Ol-9	9.40	78.7	9	-0.323	0.029	-0.502	0.050	-0.07	0.06	-0.14	0.06
Ol-10	1.19	75.7	9	-0.268	0.029	-0.411	0.050	-0.10	0.06	-0.19	0.06
Ol-11	7.08	78.3	9	-0.271	0.029	-0.413	0.050	-0.10	0.06	-0.18	0.06
Ol-12	1.36	77.0	9	-0.293	0.029	-0.439	0.050	-0.09	0.06	-0.17	0.06
Ol-13	1.44	77.6	9	-0.180	0.029	-0.258	0.050	-0.11	0.05	-0.23	0.06
Ol-14	0.31	76.9	9	-0.210	0.029	-0.321	0.050	-0.15	0.05	-0.26	0.06
Ol-15	0.72	77.9	9	-0.306	0.029	-0.480	0.050	-0.11	0.05	-0.19	0.06
Ol-16	0.40	79.7	9	-0.321	0.025	-0.454	0.051	-0.10	0.05	-0.16	0.06
Ol-17	0.49	76.9	9	-0.316	0.025	-0.473	0.051	-0.10	0.05	-0.20	0.06
Ol-18	1.28	78.7	9	-0.164	0.025	-0.278	0.051	-0.11	0.05	-0.25	0.06
Ol-19	0.51	75.4	9	-0.226	0.025	-0.368	0.051	-0.11	0.05	-0.25	0.06
Ol-20	0.62	81.3	9	-0.205	0.025	-0.316	0.051	-0.10	0.05	-0.25	0.06
Ol-21	0.47	77.0	9	-0.240	0.025	-0.374	0.051	-0.12	0.05	-0.20	0.06
Ol-22	1.02	78.0	9	-0.238	0.025	-0.401	0.051	-0.09	0.05	-0.19	0.06
<i>T4D4-01</i>											
Ol-1	3.48	87.4	9	-0.012	0.023	-0.023	0.042	-0.14	0.05	-0.30	0.06
Column 2×								-0.15	0.06	-0.32	0.09
Ol-2	4.15	86.5	9	0.489	0.023	0.716	0.042	-0.19	0.05	-0.40	0.06
Column 2×								-0.23	0.06	-0.43	0.09
Ol-3	0.9	86.1	9	-0.208	0.023	-0.304	0.042	-0.12	0.05	-0.25	0.06
Ol-4	0.68	86.9	9	0.018	0.023	0.000	0.042	-0.13	0.06	-0.30	0.09
Ol-5	0.57	88.3	9	0.041	0.023	0.053	0.042	-0.13	0.06	-0.28	0.09
Ol-6	0.57	88.2	9	0.072	0.023	0.088	0.042	-0.15	0.06	-0.29	0.09
Ol-7	0.34	87.3	9	0.239	0.023	0.343	0.042	-0.15	0.06	-0.33	0.09
Ol-8	5.39	87.4	5	0.095	0.035	0.087	0.059	-0.15	0.06	-0.29	0.09
Ol-9	3.44	86.6	5	0.199	0.035	0.263	0.059	-0.17	0.06	-0.31	0.09
Ol-10	2.41	88.1	5	0.021	0.035	0.043	0.059	-0.15	0.06	-0.29	0.08
Ol-11	2.82	85.3	5	0.354	0.035	0.503	0.059	-0.18	0.06	-0.38	0.08
Ol-12	0.57	89.2	5	0.035	0.035	0.056	0.059	-0.11	0.06	-0.25	0.08
Ol-13	2.08	88.3	5	0.078	0.035	0.059	0.059	-0.14	0.06	-0.27	0.08
Ol-14	1.19	88.0	5	0.107	0.035	0.085	0.059	-0.16	0.06	-0.31	0.08
Ol-15	3.29	87.4	5	0.030	0.035	0.021	0.059	-0.15	0.05	-0.27	0.07
<i>T4D2#1</i>											
Ol-1	1.69	87.3	9	0.082	0.025	0.107	0.044	-0.16	0.04	-0.29	0.06
Replicate			6	0.078	0.034	0.111	0.056				
Ol-2	1.85	88.3	8	0.020	0.023	0.009	0.038	-0.15	0.04	-0.30	0.06
Ol-3	0.9	85.7	9	0.124	0.025	0.165	0.044	-0.18	0.04	-0.34	0.06

(continued on next page)

**Table 1** (continued)

Sample	wt. (mg)	Fo	n	$\delta^{56}\text{Fe}$ (‰)	95% c.i.	$\delta^{57}\text{Fe}$ (‰)	95% c.i.	$\delta^{25}\text{Mg}$ (‰)	2 SD	$\delta^{26}\text{Mg}$ (‰)	2 SD
Ol-4	2.86	88.6	8	0.054	0.023	0.068	0.038	-0.16	0.04	-0.29	0.06
Ol-5	0.79	87.3	9	0.041	0.025	0.030	0.044	-0.15	0.04	-0.31	0.06
Ol-6		88.1						-0.14	0.05	-0.31	0.07
Ol-7	0.65	88.9	9	0.153	0.025	0.171	0.044	-0.15	0.05	-0.31	0.07
Ol-8		87.7						-0.16	0.05	-0.33	0.07
Ol-9	0.95	88.7	6	0.128	0.034	0.177	0.056	-0.16	0.05	-0.29	0.07
Ol-10	0.58	87.0	6	0.157	0.034	0.204	0.056	-0.17	0.05	-0.34	0.07
<i>KOO-17A</i>											
Ol-1	0.44	87.9	8	0.117	0.023	0.162	0.038	-0.15	0.05	-0.30	0.07
Ol-2		88.4						-0.14	0.05	-0.28	0.07
Ol-3		88.5						-0.14	0.05	-0.26	0.07
Ol-4		87.4						-0.12	0.05	-0.29	0.07
Ol-5	0.52	87.0	9	0.165	0.025	0.238	0.044	-0.18	0.05	-0.31	0.07
Ol-6	0.4	87.2	9	0.179	0.025	0.235	0.044	-0.17	0.06	-0.33	0.09
Ol-7	0.28	87.0	8	0.172	0.023	0.224	0.038	-0.15	0.04	-0.30	0.06
Ol-8	0.4	87.0	8	0.145	0.023	0.196	0.038	-0.15	0.04	-0.31	0.06
Ol-9	0.4	87.0	9	-0.040	0.025	-0.087	0.044	-0.13	0.04	-0.28	0.06
Ol-10	0.6	87.2	8	0.008	0.023	-0.021	0.038	-0.16	0.04	-0.30	0.06

Fo = molar  $100 \times \text{Mg} / (\text{Mg} + \text{Fe})$ , with an uncertainty of  $\pm 0.2$ ;  $\delta^x\text{Mg} = [({}^x\text{Mg}/{}^{24}\text{Mg})_{\text{sample}} / ({}^x\text{Mg}/{}^{24}\text{Mg})_{\text{DSM3}} - 1] \times 1000$  where  $x = 25$  or  $26$ . 2 SD stands for two standard deviations of the mean for 4 replicate analyses of the same solution.  $\delta^x\text{Fe} = [({}^x\text{Fe}/{}^{54}\text{Fe})_{\text{sample}} / ({}^x\text{Fe}/{}^{54}\text{Fe})_{\text{IRMM-014}} - 1] \times 1000$  where  $x = 56$  or  $57$ . 95% c.i. stands for 95% confidence interval of the mean for  $n$  replicate analyses of the same solution and it includes the long-term reproducibility based on replicate analyses of BHVO-1 standard (Dauphas et al., 2009b). Replicate denotes repeating column chemistry and instrumental analysis. Column 2 $\times$  denotes processing sample solution through column chemistry twice. Iron isotopic data for samples KI81-5-254.5 and KI75-1-139.3 are from Teng et al. (2008).

compositions of whole-rock basalts and standards are reported in Table 2.

The isotopic compositions of two standard samples (Allende and DTS-2) analyzed during the course of this study agree well with published values (Table 2). The five whole-rock basalts have homogeneous  $\delta^{26}\text{Mg}$  (Teng et al., 2010a) and limited variation in  $\delta^{56}\text{Fe}$  that are within the ranges of typical oceanic basalts (Dauphas et al., 2009a; Poitrasson et al., 2004; Schoenberg and von Blanckenburg, 2006; Schuessler et al., 2009; Teng et al., 2008; Weyer and Ionov, 2007).

Magnesium and iron isotopes are extensively fractionated in 63 individual olivine fragments, with  $\delta^{26}\text{Mg}$  ranging from  $-0.42$  to  $+0.03\%$  and  $\delta^{56}\text{Fe}$  ranging from  $-1.10$  to  $+0.49\%$  (Fig. 1). The Fo contents of these olivine fragments also vary greatly from 75.4 to 89.2 (Fig. 2). The isotopic compositions of Mg and Fe are linearly, negatively correlated in a  $\delta^{26}\text{Mg}$  vs.  $\delta^{56}\text{Fe}$  diagram, with a slope of  $-3.3 \pm 0.3$  (Fig. 1).  $\delta^{26}\text{Mg}$  and  $\delta^{56}\text{Fe}$  values also vary with Fo content, from strong correlation as seen in sample KI81-5-254.5 to the lack of a correlation

as seen in sample KI75-1-139.3 (Fig. 2). In situ analysis of Fo content reveals the presence of strongly zoned olivines in both samples KI81-5-254.5 and KI75-1-139.3, from Kilauea Iki lava lake (Fig. 3, also see Helz, 1987b).

## 5. Discussion and conclusion

The highly variable Mg and Fe isotopic compositions of olivines from Hawaii reflect Mg and Fe isotope fractionation during differentiation of basaltic magma. In this section, we examine in detail the mechanisms that could produce such large isotope fractionations and discuss the potential petrological applications to understand magma crystallization and thermal histories.

### 5.1. Chemical diffusion-driven magnesium and iron isotope fractionation

Three processes could potentially produce Mg and Fe isotopic variations at high temperature: equilibrium isotope fractionation (Li et al., 2011; Liu et al., 2011; Polyakov et al., 2007; Schuessler et al., 2007; Shahar et al., 2008), isotope fractionation associated with Soret effect (Huang et al., 2010; Richter et al., 2008, 2009b), and kinetic isotope fractionation during chemical diffusion (Dauphas, 2007; Richter et al., 2008, 2009b; Roskosz et al., 2006).

It was speculated that Fe isotopes could be fractionated due to equilibrium fractionation between  $\text{Fe}^{2+}$  and  $\text{Fe}^{3+}$  and preferential partitioning of isotopically light Fe into olivines (Teng et al., 2008). However, this model would not predict any Mg isotope fractionation in olivine. Furthermore, the degree of equilibrium fractionation of Mg isotopes is expected to be greater than that of Fe isotopes because of their mass difference, which is consistent with studies of natural samples. For example,  $>0.55\%$  per amu fractionation of Mg isotopes occurred between clinopyroxene and garnet in eclogites (Li et al., 2011), but only  $<0.2\%$  per amu occurred for Fe isotopes (Beard and Johnson, 2004; Williams et al., 2009). Finally, large intra-mineral Mg and Fe isotopic variations are not expected during equilibrium isotope fractionation (Li et al., 2011; Liu et al., 2011; Polyakov et al., 2007; Schuessler et al., 2007; Shahar et al., 2008). All these are contrary to the observations made here and thus rule out the possibility of equilibrium isotope fractionation as causes of Mg and Fe isotopic variations in the olivines.

**Table 2**  
Magnesium and iron isotopic compositions of standards and Hawaiian basalts.

Sample	$\delta^{25}\text{Mg}$ (‰)	2 SD	$\delta^{26}\text{Mg}$ (‰)	2 SD	$\delta^{56}\text{Fe}$ (‰)	95% c. i.	$\delta^{57}\text{Fe}$ (‰)	95% c. i.
<i>Koolau, Hawaii</i>								
KOO-17A	-0.10	0.05	-0.21	0.07	-0.011	0.024	-0.017	0.046
<i>Kilauea Iki lava lake, Hawaii</i>								
KI75-1-139.3	-0.11	0.03	-0.24	0.04	+0.125	0.030	0.183	0.040
KI81-5-254.5	-0.12	0.03	-0.26	0.04	+0.111	0.038	+0.141	0.044
<i>Loihi, Hawaii</i>								
T4D4-01	-0.12	0.03	-0.24	0.04	+0.094	0.031	+0.138	0.051
T4D2#1	-0.13	0.03	-0.28	0.04	+0.047	0.030	+0.073	0.050
<i>Standards</i>								
Allende	-0.16	0.04	-0.31	0.05	-0.015	0.031	-0.013	0.050
DTS-2	-0.16	0.06	-0.33	0.05	-0.010	0.028	-0.004	0.045

Magnesium isotopic data of whole-rock basalts are from Teng et al. (2010a). 95% c.i. stands for 95% confidence interval of the mean for 9 replicate analyses of the same solution and it includes the long-term reproducibility based on replicate analyses of BHVO-1 standard (Dauphas et al., 2009b).

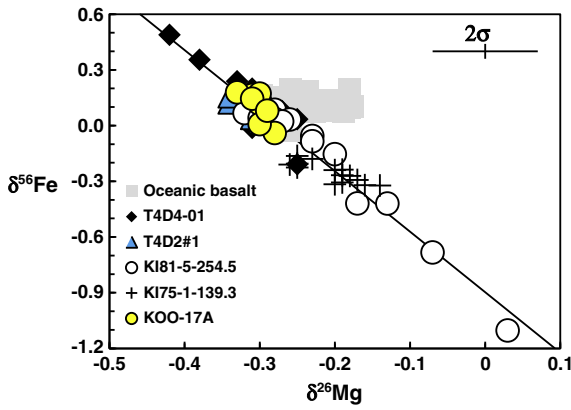


**Fig. 1.** Mg and Fe isotope fractionations in olivine fragments from Hawaiian lavas. The data define a linear relationship with a slope of  $-3.3 \pm 0.3$  (solid line). Olivine data are reported in Table 1. Oceanic basalt data are reported in Table 2 and Teng et al. (2008, 2010a).

Both Mg and Fe isotopes can be extensively fractionated during Soret diffusion, with light Mg and Fe isotopes preferentially concentrated at the hot end relative to the cold end of a thermal gradient (Huang et al., 2010; Richter et al., 2008, 2009b). Hence a positive correlation between  $\delta^{26}\text{Mg}$  and  $\delta^{56}\text{Fe}$  would be expected for this process. The observed negative correlation thus rules out Soret diffusion as causes of the large Mg and Fe isotopic variations in the olivines.

Instead, several lines of evidence suggest chemical diffusion as causes of the large Mg and Fe isotope fractionations in these olivines.

During inter-diffusion of Mg and Fe in olivines, Mg and Fe form a solid solution (from the end-members forsterite to fayalite), and diffusion of Fe from the melt into the olivine phenocrysts is coupled with diffusion of Mg out of the olivine phenocrysts. Since light isotopes of one element always diffuse faster than heavy ones during chemical diffusion (Dauphas, 2007; Richter et al., 2008, 2009b; Roskosz et al., 2006), a negative correlation between Mg and Fe isotopes is expected before the system reaches equilibrium (Dauphas

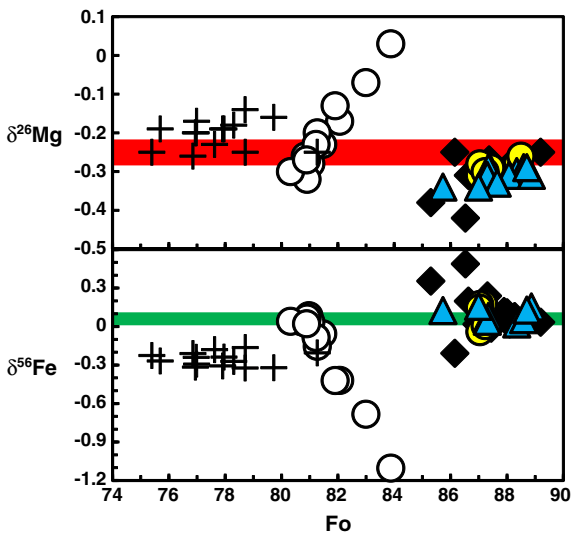


**Fig. 2.** Plots of  $\delta^{26}\text{Mg}$  and  $\delta^{56}\text{Fe}$  with Fo in olivine fragments from Hawaiian lavas. Color shielded field in each panel represents the range of whole-rock isotopic composition. Symbols as in Fig. 1. Data are reported in Tables 1 and 2.

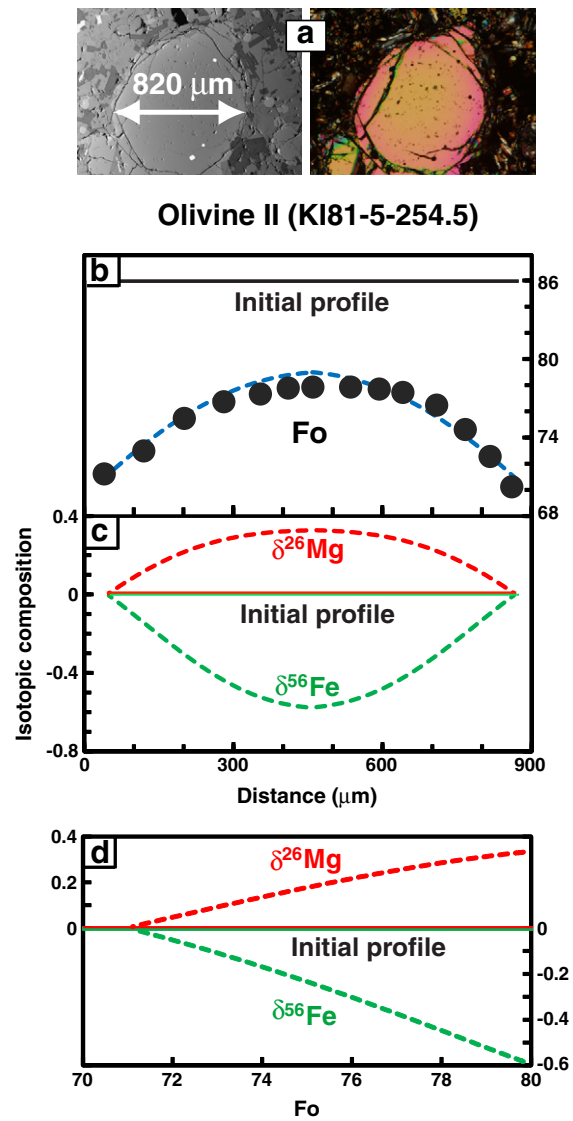


**Fig. 3.** a) Photomicrograph and backscattered electron image of an olivine phenocryst in a groundmass of plagioclase, pyroxene and olivine from sample KI81-5-254.5. The arrow marks the location of the electron microprobe traverse. b) Measured Fo variation along the traverse in the olivine phenocryst on the top panel and theoretically reproduced diffusion curve (dotted line) by Mg–Fe inter-diffusion between olivines and melts. c) Predicted Mg and Fe isotope fractionation along the traverse induced by the inter-diffusion. The solid lines are initial conditions and dotted curves are calculated spherical diffusion profiles. d) Predicted correlations of  $\delta^{26}\text{Mg}$  and  $\delta^{56}\text{Fe}$  with Fo content (dotted curves) along the traverse. The solid lines are initial conditions. Electron microprobe data are reported in the online Supplementary file. See text for modeling details.

et al., 2010). The slope of  $-3.3$  in a  $\delta^{26}\text{Mg}$  vs.  $\delta^{56}\text{Fe}$  diagram (Fig. 1) is similar to the theoretical ratio of  $-2.7$  for binary diffusion, calculated based on inter-diffusion of Mg–Fe in olivine (Dauphas et al., 2010) by assuming  $\beta_{\text{Mg}} = \beta_{\text{Fe}} = 0.05$  in the parameterization of diffusion-driven mass fractionation  $D_2/D_1 = (m_1/m_2)^{\beta}$  (Richter et al., 2008) and using an initial olivine composition of  $\text{Fo}_{86}$  (Helz, 1987b).

Olivine samples collected by drilling cores from Kilauea Iki lava lake are all normally zoned, with olivines from samples quenched at lower temperature more Fe-rich than those from samples quenched at higher temperature (Helz, 1987b; Teng et al., 2008), which directly reflects re-equilibration of the olivines with evolving residual melts. Electron probe analysis of samples studied here also reveals large compositional zoning in olivines (Table S1). The Fo zoning profile measured in a single olivine phenocryst from sample KI81-5-254.5

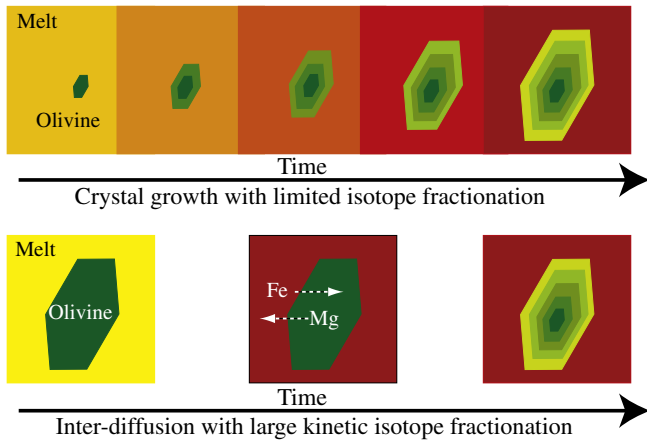


**Fig. 4.** Illustration of how crystal growth attending magmatic differentiation and inter-diffusion of Mg and Fe can affect crystal zoning (different colors represent different chemical compositions). Zoned olivine growing exclusively from evolving melt (top) is associated with limited diffusion, hence should have limited isotope fractionation. Mineral zoning in this case cannot provide constraints on the timescales of magmatic processes. By contrast, zoned olivine that is exclusively produced by inter-diffusion of Mg and Fe, due to change in the Fo content at the boundary, should produce negatively coupled Mg and Fe isotope fractionation. Olivine phenocrysts studied here show diffusive Mg–Fe exchange (bottom case).

(Fig. 3a), a drilling core sample from Kilauea Iki lava lake, can be reproduced by Mg–Fe inter-diffusion between olivines and melts (Fig. 3b). Although in-situ isotopic data are not available for these olivines, we compare measured data on different olivine fragments with theoretical predications for diffusion within an olivine phenocryst to test whether the large fractionations are produced by Mg–Fe inter-diffusion or not. More detailed comparison will await in situ determination of isotopic zoning profiles. First, the predicted isotope fractionations associated with the diffusion for the specific olivine from sample KI81-5-254.5 (Fig. 3c), are comparable to those measured in the olivine fragments (e.g., +0.3‰  $\delta^{26}\text{Mg}$  and  $-0.6\text{‰}$   $\delta^{56}\text{Fe}$  at the core of the modeled olivine). Second, the predicted correlations of  $\delta^{26}\text{Mg}$  and  $\delta^{56}\text{Fe}$  with Fo content for the specific olivine from sample KI81-5-254.5 (Fig. 3d) mimic the olivine fragment data from sample KI81-5-254.5 (Fig. 2). Finally, when compared to whole-rock isotopic compositions, olivine fragments are heavier in terms of Mg isotopes and lighter in terms of Fe isotopes for samples from Kilauea Iki lava lake, consistent with the observed normal zoning in olivines formed during re-equilibration of the olivines with evolving residual melts (Helz, 1987b; Teng et al., 2008). By contrast, more olivine fragments from Loihi have lighter Mg isotopic composition and heavier Fe isotopic composition than their whole-rock basalts. The opposite behavior between Kilauea and Loihi samples may reflect different types of zoning and magmatic differentiation processes.

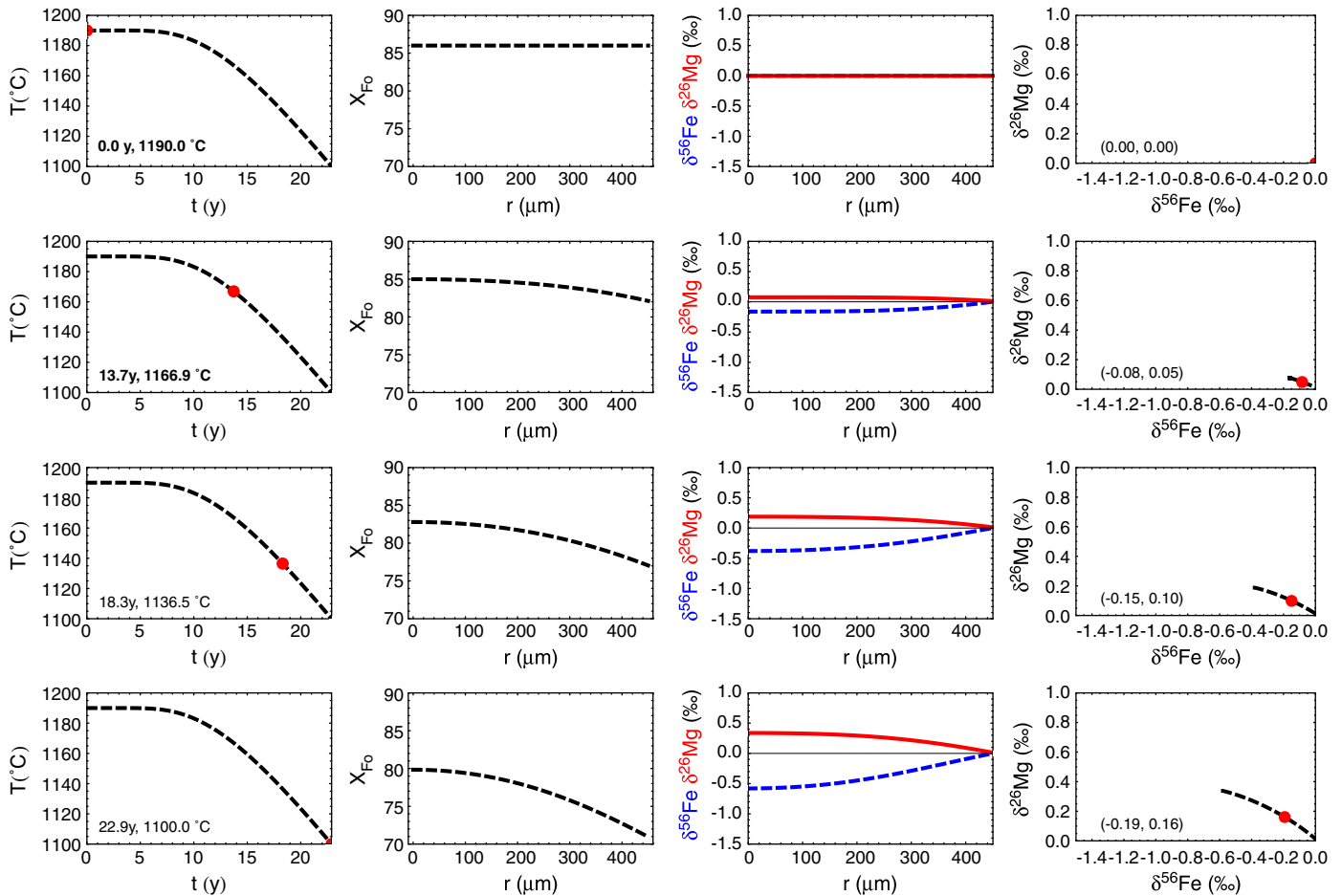


**Fig. 5.** Modeling of isotope fractionations associated with Fe–Mg inter-diffusion in olivine (the Mathematica code and an animated gif version of this figure are available in Electronic annex. See text for modeling details). The left column shows the evolution of temperature with time in the system. At a given time (shown by the red dot in the left column), the second column from the left shows the evolution of Fo content versus radial distance; the third column shows  $\delta^{26}\text{Mg}$  (solid red) and  $\delta^{56}\text{Fe}$  (dashed blue) versus radial distance and the fourth column shows  $\delta^{26}\text{Mg}$  versus  $\delta^{56}\text{Fe}$  along a profile (the bulk compositions of the olivine is shown as a red dot and is given in parentheses).

## 5.2. Implications on crystallization and thermal histories of Hawaiian magmas

Diffusive processes can constrain the timescales of geological processes like erosion, sediment burial, metamorphism and magma cooling (Muller et al., 2010; Reiners and Brandon, 2006). Olivine is ubiquitous in mafic and ultramafic rocks and can display chemical zoning indicative of disequilibrium conditions with the host magma (Costa et al., 2008; Milman-Barris et al., 2008). Such zoning can yield information on the source, magma transport, and crystallization history of basaltic magmas (Van Kooten and Buseck, 1978). However, meaningful interpretation of zoning is often hampered by the fact that it cannot be unambiguously ascribed to a single process. For example, zoned olivine can either be the result of growth from an evolving melt during magmatic differentiation or be exclusively produced by inter-diffusion of Mg and Fe (Fig. 4). Mineral zoning in the former case can provide constraints on the crystallization history of the magma but not on the timescales of magmatic processes whereas the latter case provides the opposite information. Obviously, intermediate and more complex situations may exist, where zoning produced by magmatic differentiation is partially obliterated by diffusion. It is therefore important to identify what the contribution of each process is to the observed zoning profile before making any interpretation regarding cooling and crystallization histories.

Studies of Mg and Fe isotopes can unambiguously tease apart the roles of crystal growth vs. Mg–Fe inter-diffusion that can both create zoned crystals. Zoning generated by crystal growth attending magmatic evolution should show limited isotope fractionation as equilibrium isotope fractionation between olivines and melts at high temperature is small, whereas chemical diffusion-controlled zoning is accompanied with large and negatively correlated Mg and Fe isotope fractionation (Dauphas et al., 2010). Our study indicates that normal zoning in olivine phenocrysts from Kilauea Iki lava lake is mainly produced by inter-diffusion of Mg and Fe between olivines and evolving melts. The zoning hence can be used to constrain the cooling rate of the lava lake. The total cooling time derived from modeling the diffusion profile of Mg and Fe in olivines from Kilauea Iki lava lake is ~20 years (Fig. 5), which corresponds approximately to the time span between eruption in 1959 and recovery of the quenched samples in 1981. It is worth mentioning that considerable uncertainties are associated with model calculations in the time–temperature evolution, the parameterization of the Mg–Fe inter-diffusion coefficient, and the orientation of the olivine samples analyzed. Therefore, the modeling results are not unique.

Our studies demonstrate the usefulness of in situ isotopic measurements using laser-ablation MC-ICPMS or SIMS as this will help to determine the nature of mineral zoning in igneous rocks and possibly in metamorphic rocks that are routinely measured using electron probes. The diffusion-controlled zoning can then be used to constrain the residence times of crystals in magmas and the duration of metamorphic events by modeling the diffusion profiles. Studies of Mg and Fe isotope fractionation can also be used to identify core olivine compositions that may have been affected by diffusion, where Fo content cannot be used to estimate the composition of the primary melt as is often done (Herzberg et al., 2007).

## Acknowledgement

We thank Frank Richter, Wei Yang, Wang-Ye Li, Corliss Sio, Shan Ke and Sheng-Ao Liu for discussions and Jing-Liang Guo for help with microprobe analyses. The paper benefited from constructive and detailed comments of Helen Williams and an anonymous reviewer, and efficient editing from Rick Carlson. This work was supported by NSF (EAR-0838227 and EAR-1056713) and Arkansas Space Grant Consortium (SW19002) to FZT; NSF (EAR-0820807), NASA (NNX09AG59G) and a Packard fellowship to N.D.; NSF (EAR-0951487) to SH; as well as

the NSF of China (40821061) and the Ministry of Education of China (B07039) to SG.

## Appendix A. Supplementary data

Supplementary data to this article can be found online at doi:10.1016/j.epsl.2011.06.003.

## References

- Barth, G.A., Kleinrock, M.C., Helz, R.T., 1994. The magma body at Kilauea Iki lava lake: potential insights into mid-ocean ridge magma chamber. *J. Geophys. Res.* 99 (B4), 7199–7217.
- Beard, B.L., Johnson, C.M., 2004. Inter-mineral Fe isotope variations in mantle-derived rocks and implications for the Fe geochemical cycle. *Geochim. Cosmochim. Acta* 68 (22), 4727–4743.
- Chou, I.-M., 1987. Oxygen buffer and hydrogen sensor techniques at elevated pressures and temperatures. In: Ulmer, G.C., Barnes, H.L. (Eds.), *Hydrothermal Experimental Techniques*. John Wiley & Sons, New York, pp. 61–99.
- Costa, F., Dohmen, R., Chakraborty, S., 2008. Time scales of magmatic processes from modeling the zoning patterns of crystals. *Rev. Mineral. Geochem.* 69, 545–594.
- Dauphas, N., 2007. Diffusion-driven kinetic isotope effect of Fe and Ni during formation of the Widmanstätten pattern. *Meteorit. Planet. Sci.* 42 (9), 1597–1613.
- Dauphas, N., Janney, P.E., Mendybaev, R.A., Wadhwa, M., Richter, F.M., Davis, A.M., van Zuilen, M., Hines, R., Foley, C.N., 2004. Chromatographic separation and multi-collection-ICPMS analysis of iron. Investigating mass-dependent and -independent isotope effects. *Anal. Chem.* 76 (19), 5855–5863.
- Dauphas, N., Craddock, P.R., Asimow, P.D., Bennett, V.C., Nutman, A.P., Ohnenstetter, D., 2009a. Iron isotopes may reveal the redox conditions of mantle melting from Archean to Present. *Earth Planet. Sci. Lett.* 288 (1–2), 255–267.
- Dauphas, N., Pourmand, A., Teng, F.-Z., 2009b. Routine isotopic analysis of iron by HR-MC-ICPMS: how precise and how accurate? *Chem. Geol.* 267, 175–184.
- Dauphas, N., Teng, F.-Z., Arndt, N.T., 2010. Magnesium and iron isotopes in 2.7 Ga Alexo komatiites: mantle signatures, no evidence for Soret diffusion, and identification of diffusive transport in zoned olivine. *Geochim. Cosmochim. Acta* 74, 3274–3291.
- Dohmen, R., Chakraborty, S., 2007. Fe–Mg diffusion in olivine II: point defect chemistry, change of diffusion mechanisms and a model for calculation of diffusion coefficients in natural olivine (vol 34, pg 409, 2007). *Phys. Chem. Miner.* 34, 597–598.
- Helz, R.T., 1987a. Differentiation behavior of Kilauea Iki lava lake, Kilauea Volcano, Hawaii: an overview of past and current work. In: Mysen, B.O. (Ed.), *Magmatic Processes: Physicochemical Principles: Geochem. Soc. Spec. Publ.*, 1, pp. 241–258.
- Helz, R.T., 1987b. Diverse olivine types in lava of the 1959 eruption of Kilauea volcano and their bearing on eruption dynamics. *U.S.G.S. Prof. Paper*, 1350, pp. 691–722.
- Helz, R.T., 2009. Processes active in mafic magma chambers: the example of Kilauea Iki lava lake, Hawaii. *Lithos* 111, 37–46.
- Helz, R.T., Thornber, C.R., 1987. Geothermometry of Kilauea Iki lava lake, Hawaii. *Bull. Volcanol.* 49, 651–668.
- Herd, C.D.K., 2008. Basalts as probes of planetary interior redox state. *Rev. Mineral. Geochem.* 68, 527–553.
- Herzberg, C., Asimow, P.D., Arndt, N.T., Niu, Y., Leshner, C.E., Fitton, J.G., Cheadle, M.J., Saunders, A.D., 2007. Temperatures in ambient mantle and plumes: constraints from basalts, picrites, and komatiites. *Geochem. Geophys. Geosyst.* 8 (2), Q02006. doi:10.1029/2006GC001390.
- Huang, F., Chakraborty, P., Lundstrom, C.C., Holmden, C., Glessner, J.J.G., Kieffer, S.W., Leshner, C.E., 2010. Isotope fractionation in silicate melts by thermal diffusion. *Nature* 464, 396–400.
- Huebner, J.S., Sato, M., 1970. The oxygen fugacity–temperature relationships of manganese oxide and nickel oxide buffers. *Am. Mineral.* 55, 934–952.
- Li, W.-Y., Teng, F.-Z., Ke, S., Rudnick, R.L., Gao, S., Wu, F.-Y., Chappell, B.W., 2010. Heterogeneous magnesium isotopic composition of the upper continental crust. *Geochim. Cosmochim. Acta* 74, 6867–6884.
- Li, W.-Y., Teng, F.Z., Xiao, Y., Huang, J., 2011. High-temperature inter-mineral magnesium isotope fractionation in eclogite from the Dabie orogen, China. *Earth Planet. Sci. Lett.* 304, 224–230.
- Liu, S.-A., Teng, F.-Z., He, Y., Ke, S., Li, S., 2010. Investigation of magnesium isotope fractionation during granite differentiation: implication for Mg isotopic composition of the continental crust. *Earth Planet. Sci. Lett.* 297, 646–654.
- Liu, S.-A., Teng, F.Z., Yang, W., Wu, F.Y., 2011. High-temperature inter-mineral magnesium isotope fractionation in mantle xenoliths from the North China craton. *Earth Planet. Sci. Lett.* 308, 131–140.
- Milman-Barris, M.S., Beckett, J.R., Baker, M.B., Hofmann, A.E., Morgan, Z., Crowley, M.R., Vielzeuf, D., Stolper, E.M., 2008. Zoning of phosphorus in igneous olivine. *Contrib. Mineral. Petrol.* 155, 739–765.
- Muller, T., Watson, E.B., Harrison, T.M., 2010. Applications of diffusion data to high-temperature Earth systems. *Rev. Mineral. Geochem.* 72, 997–1038.
- Poitrasson, F., Halliday, A.N., Lee, D.C., Levasseur, S., Teutsch, N., 2004. Iron isotope differences between Earth, Moon, Mars and Vesta as possible records of contrasted accretion mechanisms. *Earth Planet. Sci. Lett.* 223 (3–4), 253–266.
- Polyakov, V.B., Clayton, R.N., Horita, J., Mineev, S.D., 2007. Equilibrium iron isotope fractionation factors of minerals: reevaluation from the data of nuclear inelastic resonant X-ray scattering and Mossbauer spectroscopy. *Geochim. Cosmochim. Acta* 71 (15), 3833–3846.

- Reiners, P.W., Brandon, M.T., 2006. Using thermochronology to understand orogenic erosion. *Annu. Rev. Earth Planet. Sci.* 34, 419–466.
- Richter, F.M., Watson, E.B., Mendybaev, R.A., Teng, F.-Z., Janney, P.E., 2008. Magnesium isotope fractionation in silicate melts by chemical and thermal diffusion. *Geochim. Cosmochim. Acta* 72, 206–220.
- Richter, F.M., Dauphas, N., Teng, F.-Z., 2009a. Non-traditional fractionation of non-traditional isotopes: evaporation, chemical diffusion and Soret diffusion. *Chem. Geol.* 258, 92–103.
- Richter, F.M., Watson, E.B., Mendybaev, R.A., Dauphas, N., Georg, R.B., Watkins, J., Valley, J.W., 2009b. Isotopic fractionation of the major elements of molten basalt by chemical and thermal diffusion. *Geochim. Cosmochim. Acta* 73, 4250–4263.
- Roskosz, M., Luais, B., Watson, H.C., Toplis, M.J., Alexander, C.M.O.D., Mysen, B.O., 2006. Experimental quantification of the fractionation of Fe isotopes during metal segregation from a silicate liquid. *Earth Planet. Sci. Lett.* 248, 851–867.
- Schoenberg, R., von Blanckenburg, F., 2006. Modes of planetary-scale Fe isotope fractionation. *Earth Planet. Sci. Lett.* 252 (3–4), 342–359.
- Schuessler, J.A., Schoenberg, R., Behrens, H., von Blanckenburg, F., 2007. The experimental calibration of the iron isotope fractionation factor between pyrrhotite and peralkaline rhyolitic melt. *Geochim. Cosmochim. Acta* 71 (2), 417–433.
- Schuessler, J.A., Schoenberg, R., Sigmarsson, O., 2009. Iron and lithium isotope systematics of the Hekla volcano, Iceland – evidence for Fe isotope fractionation during magma differentiation. *Chem. Geol.* 258 (1–2), 78–91.
- Shahar, A., Manning, C.E., Young, E.D., 2008. Equilibrium high-temperature Fe isotope fractionation between fayalite and magnetite: an experimental calibration. *Earth Planet. Sci. Lett.* 268, 330–338.
- Teng, F.-Z., Wadhwa, M., Helz, R.T., 2007. Investigation of magnesium isotope fractionation during basalt differentiation: implications for a chondritic composition of the terrestrial mantle. *Earth Planet. Sci. Lett.* 261 (1–2), 84–92.
- Teng, F.-Z., Dauphas, N., Helz, R.T., 2008. Iron isotope fractionation during magmatic differentiation in Kilauea Iki lava lake. *Science* 320, 1620–1622.
- Teng, F.-Z., Li, W.-Y., Ke, S., Marty, B., Dauphas, N., Huang, S., Wu, F.-Y., Pourmand, A., 2010a. Magnesium isotopic composition of the Earth and chondrites. *Geochim. Cosmochim. Acta* 74, 4150–4166.
- Teng, F.-Z., Li, W.-Y., Rudnick, R.L., Gardner, L.R., 2010b. Contrasting behavior of lithium and magnesium isotope fractionation during continental weathering. *Earth Planet. Sci. Lett.* 300, 63–71.
- Van Kooten, G.K., Buseck, P.R., 1978. Interpretation of olivine zoning: study of a maar from the San Francisco volcanic field, Arizona. *Geol. Soc. Am. Bull.* 89, 744–754.
- Weyer, S., Ionov, D.A., 2007. Partial melting and melt percolation in the mantle: the message from Fe isotopes. *Earth Planet. Sci. Lett.* 259, 119–133.
- Williams, H.M., McCammon, C.A., Peslier, A.H., Halliday, A.N., Teutsch, N., Levasseur, S., Burg, J.P., 2004. Iron isotope fractionation and the oxygen fugacity of the mantle. *Science* 304 (5677), 1656–1659.
- Williams, H.M., Peslier, A.H., McCammon, C., Halliday, A.N., Levasseur, S., Teutsch, N., Burg, J.P., 2005. Systematic iron isotope variations in mantle rocks and minerals: the effects of partial melting and oxygen fugacity. *Earth and Planetary Science Letters* 235 (1–2), 435–452.
- Williams, H.M., et al., 2009. Fractionation of oxygen and iron isotopes by partial melting processes: implications for the interpretation of stable isotope signatures in mafic rocks. *Earth and Planetary Science Letters* 283, 156–166.
- Yang, W., Teng, F.-Z., Zhang, H.-F., 2009. Chondritic magnesium isotopic composition of the terrestrial mantle: a case study of peridotite xenoliths from the North China Craton. *Earth and Planetary Science Letters* 288 (3–4), 475–482.